INFLUENCE OF INTERORBIT ACCELERATION ON THE DESIGN OF LARGE SPACE ANTENNAS

John M. Hedgepeth
Astro Research Corporation

INTRODUCTION

Large antennas in space will eventually be needed. Not only will satellite-based communications require antennas of 100 meters or more in diameter but also will remote sensing demand even larger sizes. Some of the predicted needs are characterized in Figure 1, taken from ref. 1. Other studies predict even larger apertures.

Most of the envisioned missions involve orbits that are inaccessible to the Space Shuttle itself. Accordingly, the design of the antenna structure must either countenance automated remote deployment in the operational orbit or must include the loadings due to interorbit boost in the structural requirements of the erected antenna. The purpose of this paper is to investigate, in general, the characteristics of the acceleration-induced loading in structures consisting of triangular lattices and to present some initial quantitative results on the effect on the design mass and stowage volume.

The approach herein is to define the structural design that would be used if no interorbit acceleration were required and then to determine what strengthening would be required to accommodate the loads due to acceleration. The basic zero-acceleration design can be based on the stringent accuracy requirements placed on the antennas.

The missions shown in Figure 1 are seen to involve ratios of diameter to wavelength up to more than 100,000 with the majority centered around a ratio of 1,000. For those missions for which the main beam must contain almost all the radiated energy, the emitted wave front must be accurate to 4 percent of the wavelength. These

missions include all the earth-directed antennas in which side-lobe gain must be kept very low. Even in the cases wherein side-lobe gain is of primary importance, the rms errors in the wave front are held to less than 12 percent of the wavelength. These missions include outward-pointed antennas for which the side-lobe gain can be relatively large.

In a reflector antenna, the wave-front error is very nearly twice the component of structural distortion normal to the reflector surface. Thus, the surface error of a reflector antenna must be held to one-fiftieth of a wavelength for the low-side-lobe missions and one-sixteenth of a wavelength for the high-gain missions.

Combining the foregoing relationships with the data in Figure 1 yields the requirement on structural surface accuracy. Submillimeter radio astronomy, for example, requires an accuracy of one part per million of the diameter. Those earthward-pointed missions which have a diameter wavelength ratio of around 1,000 require a surface accuracy of 20 parts per million. At the other end, low-frequency radio astronomy allows the surface error to be as much as one-thousandth of the diameter.

STRUCTURAL CONFIGURATIONS

The type of spacecraft under consideration is shown in the center of Figure 2. It consists of a reflector and a radiofrequency feed mounted at a distance by some sort of structure. Of course, the feed position and orientation with respect to the reflector is important, but in this paper attention is confined to the reflector portion only.

Four reflector configurations are shown in Figure 2 and in more detail in Figures 3 through 6. These four are selected to encompass the types that utilize a knitted mesh material for the actual reflector surface. Such material packages very well, is lightweight (~50 g/m^2), is compliant, and only needs to be positioned properly to be an excellent reflector.

The tetrahedral truss has been discussed by many authors. Differences exist in scale and in the manner in which the structure

and the mesh interface. In the form treated herein, the interface with the mesh is only at the triangular lattice nodes. Separate tendons under high tension are laced through the mesh along lines parallel to the surface truss elements and attached at the nodes. The structural members therefore must carry only axial compression and tension and can thus be slender for lightly loaded situations. Properly located joints allow stowage and deployment of the otherwise uncompliant structure. From an overall standpoint, the tetrahedral truss structure can be thought of as a thick shell, the surface of which is defined by the lattice nodes. For the equilateral triangular geometry, the shell is isotropic, an advantage that does not obtain for some of the other truss geometries proposed.

The geodesic dome can be viewed as the limiting case of a tetrahedral truss as the thickness H is reduced to zero. The geodesic dome behaves in the large as a membrane. It is simpler than the truss since only one surface of lattice elements is required. On the other hand, the membrane-like surface is very flexible unless the edge is supported by a stiff ring. Packaging and deploying the ring may present more difficulties than those presented by the more nearly uniform tetrahedral truss. The interface with the mesh is again assumed to be at the lattice nodes and the structural members carry axial tension and compression only.

The radial-rib configuration has as its structure a large number of radially oriented curved beams that are cantilevered from the central hub. The interface with the reflecting mesh is continuous along the chords of the beams. Thus the mesh is in gores rather than facets as is the case for the other configurations. The beams are stowed by wrapping them around the central hub with the necessary compliance supplied in a number of ways. The ATS-6 antenna is a salient example of this configuration.

The pretensioned truss is the author's version of the variously named "Maypole," "Hoop-and-Column," "Wire-Wheel," and "Spoked-Wheel" concepts. The basic structural element is the bicycle-wheel structure made up of the central column (hub) and the compression rim tied together by stays. The rim is articulated, allowing stowage.

The central column is an Astromast. The rest of the structure is "soft" in the sense that its elements need to carry tension only. Thus a variety of packaging techniques can be used without requiring complex joints. On the other hand, the deployed structure is "stiff." The tension-carrying elements are pretensioned sufficiently to allow incremental compression loading in orbit while still retaining positive tension. The front and back stays, for example, thus maintain their full axial stiffness.

The reflector surface is formed by structural tension-stiffened radial beams. The tension in the curved chords automatically pretension the interchord members. The chord pretension is reacted by the compression rim. A compression spreader is needed at the outer end. The pretensioned beam is cantilevered at the central hub and also supported at the tip by the rim. Circumferential tension members provide the remainder of the structure. They and the upper chords of the beams are laced through the mesh to provide the necessary shaping to the reflector surface in quadrilateral facets.

MESH SADDLING

Since the mesh has no bending stiffness, it behaves like a membrane; it can carry no compression. Furthermore, the tension must be sensible and reasonably uniform and isotropic in order to assure good electrical conductivity (and, hence, rf reflectivity) of the mesh. Values of around 2.5 N/m are used, for example, in the Harris studies in ref. 2.

A biaxially tensioned membrane with no lateral loading must have zero Gaussian curvature. Thus if the curvature in one direction is positive, the curvature in the other direction must be negative. Desired reflector surfaces are approximately spherical with a radius of curvature of twice the focal length F. Unfortunately, mesh surfaces want to look like saddles.

For a faceted reflector configuration, the best approximation to a dish is to make the facets flat, with the corners located so

as to cancel the average deviation between the flat and the desired curved surface. The rms deviation is kept small enough by limiting the size of the facets.

At the intersection between adjacent facets, the tension in the mesh changes direction. This produces a slight bow of the supporting tendon laced through the mesh as illustrated in Figure 7. The deviation between the saddled mesh surface and the desired spherical surface is

$$w = \frac{1}{12F}\left\{\frac{\ell^2}{4} - 3x^2 - 3y^2 + \frac{2N}{T}\left[\frac{\sqrt{3}}{90}\,\ell^3 + x(x^2 - 3y^2)\right]\right\}$$

where x and y are Cartesian coordinates with origin at the center of the triangle and the negative x axis passing through a vertex. The mesh tension per unit length is N and the tendon tension is T. The corresponding rms deviation divided by the antenna diameter is

$$\frac{w_{rms}}{D} = 0.01614\,\frac{(\ell/D)^2}{F/D}\left(1 + 0.33\,\frac{N\ell}{T}\right)$$

In order to allow the largest facet size, the tendon tension must be large, say greater than 10 $N\ell$. Then the facet size for an allowable value of rms deviation is

$$\frac{\ell}{D} = 7.87\sqrt{\frac{F}{D}\left(\frac{w_{rms}}{D}\right)_{Allow.}}$$

for the triangular facet.

If the facets are rectangular, the same process yields

$$\frac{w_{rms}}{D} = 0.0186\,\frac{(\ell/D)^2}{F/D}\sqrt{1 + \left(\frac{b}{\ell}\right)^4}\left[1 + C\left(\frac{b}{\ell}\right)\frac{N\ell}{T}\right]$$

where b is the smaller rectangle dimension, and C varies from about 0.2 to about 0.6 as b/ℓ varies from 1 to 2. Again, in order to maximize facet size, set $b < 0.5$ and $T > 10N$. Then

$$\frac{\ell}{D} = 7.33 \sqrt{\frac{F}{D}\left(\frac{w_{rms}}{D}\right)_{Allow.}}$$

for the rectangular facet.

For the radial-rib configuration, the mesh is in gores. The curvature in the radial direction is enforced to be that of the rib. The saddling produces a negative curvature in the circumferential direction equal to N_1/N_2 times the radial curvature, where N_1 and N_2 are the membrane tensions in the radial and circumferential directions, respectively (see Figure 7). The resulting rms deviation is

$$\frac{w_{rms}}{D} = 0.01076 \frac{(\ell/D)^2}{F/D}\left(1 + \frac{N_1}{N_2}\right)$$

where ℓ is the gore width at the rim. For isotropic mesh tension, $N_1 = N_2$ and

$$\frac{\ell}{D} = 6.82 \sqrt{\frac{F}{D}\left(\frac{w_{rms}}{D}\right)_{Allow.}}$$

for the gore configuration.

The facet and gore sizes are shown in Figure 8. These curves can be used to determine the required degree of refinement of the structural geometry.

EFFECT OF FABRICATION IMPERFECTIONS

Designing the geometry correctly is only the first step. The departure of the as-fabricated structure from the design must also

fall within acceptable limits. Presumably, the effects of systematic fabrication imperfections can be removed by a combination of tooling and testing. There still remains the surface error due to random imperfections.

This subject is treated in detail in ref. 3. The results are characterized in Figure 9. In this figure, the achievable ratio of diameter to wavelength is shown as a function of the standard deviation of the unit length error σ_ε of the members composing the structure for various structural configurations. Note that the radial-rib design is not included because of its much lower potential capability.

The quantity σ_ε is at the control of the designer, although with a considerable cost impact. In general, a value of σ_ε of 10^{-3} is representative of ordinary careful practice, of 10^{-4} is characteristic of a high-quality machine ship, of 10^{-5} is achievable with well designed and operated hard tooling, and of 10^{-6} is very difficult and costly.

The difficulty in achieving very small values of σ_ε can be visualized by considering to what stress levels they correspond. For example, in steel, magnesium, titanium or aluminum, the stress level corresponding to a strain of 10^{-6} is induced in only 2.5 meters of material vertically suspended in a 1-g field.

In preparing Figure 9, the criterion was established that the surface distortion shall be limited by one-half of the allowable $\lambda/50$ that is the requirement for most of the missions described in Figure 1. This is done in order to allow the various sources of error (which are, in general, additive on a mean-square basis) to coexist and still be able to meet the $\lambda/50$ requirement.

A particular ratio of focal length to diameter of two is chosen for the comparison. Most antennas with electronically steerable beams will require such a high F/D.

As can be seen in Figure 9, the tetrahedral truss is by far the most attractive configuration for attainment of large apertures

with acceptable error due to fabrication imperfections. A value of D/λ of nearly 10,000 is possible for a fabrication tolerance parameter of 10^{-5}. Reference to Figure 1 shows that this ratio would encompass all the missions except those involving submillimeter and IR astronomy. And if the relaxed $\lambda/16$ criteria were used, a value of $D/\lambda = 30,000$ would be feasible. Thus even submillimeter astronomy is possible from this standpoint.

The pretensioned truss is probably more readily packaged than the tetrahedral truss. It shows good accuracy for most of the missions.

Even the geodesic dome and a deep-rib design present usable accuracy for the smaller-aperture communication-satellite missions.

ENVIRONMENTAL STRAINS

The antenna must remain accurate in the presence of environmental effects after it is established in space. It is assumed that materials will be available with the necessary dimensional stability in the vacuum, UV, and particulate radiation environment that exists in orbit. Furthermore, it is assumed that redundant design will be used to resist the deleterious effects of the uncertainty in such strains can be kept to acceptable limits by proper design. (Indeed, this latter requirement is probably the overriding design criterion.) But there remains the ubiquitous effects of thermal strains.

The influence of thermal strains on surface accuracy is complex and dependent to a great extent on detailed design. Some overall preliminary considerations are considered in ref. 3. Attention is restricted to the tetrahedral-truss structure inasmuch as it exhibits the most potential for accurate reflectors. The results are summarized in Figure 10.

Here the ratio of diameter to wavelength is shown as a function of the maximum thermal strain parameter $\alpha_T T_{max}$, where α_T is the thermal expansion coefficient and T_{max} is the maximum radiation equilibrium temperature for a general member.

When the sun shines on a triangular grid of elements, some of them are hotter than the others because their axes are more nearly normal to the solar radiation. The differing temperatures cause differing strains in the members of differing orientation. The strains can be expressed in terms of equivalent biaxial normal and completely defined by the average strain ε_{ave} and the maximum shear strain γ_{max}. Results for the effects of average and shear strain are shown in Figure 10.

Another source of thermal gradient is the temperature difference between the two faces of the tetrahedral truss due to shading on one face by the other - and by the intersurface members. The amount of shading depends, of course, on the slenderness of the truss members. (Note that shading due to the mesh is assumed to apply uniformly to both surfaces.) The analysis is linearized with respect to d/ℓ and is therefore only accurate for low d/ℓ. It considers only shading due to the surface members. The shading due to the intersurface members is included approximately by the factor k in the expression for the strain differential.

The maximum shading effect is obtained when the sun strikes the surface perpendicular to a set of members. Total blocking is achieved for glancing illumination. Of course, this situation is unrealistic for the curved dishes under consideration. For this reason, the curves are cut off at $\theta = 80°$.

The temperature differences between surfaces could be a severe limiter on the antenna sizes for the tetrahedral truss, the effects being much more severe than either overall temperature-strain effects or shear-strain effects. For a nominal worst case of $T_{max} = 295$ K and α_T of 0.5×10^{-6}/K (readily achieved for graphite/epoxy), the limiting value of D/ℓ is 1,000. In order to achieve

the D/λ of 10,000, of which the tetrahedral truss is otherwise capable, an order of magnitude improvement would be required. This could be accomplished through a combination of deepening the truss, making the members more slender (perhaps not feasible if loading is already high), reducing the absorptivity-emissivity ratio, and finally, assuming a more stable material. Much remains to be done in this area.

LOADS DUE TO INTERORBIT ACCELERATION

Consider a tetrahedral truss dish of circular plan form which is accelerated by a thrust at its center of gravity. The thrust is applied perpendicular to the dish. For most antennas, the dish is shallow enough and the facet size is small enough that the tetrahedral truss will behave like a flat plate insofar as overall deformation and loading are concerned. The radial and circumferential bending moments so produced must be absorbed by radial and circumferential stress restraints in the upper and lower truss surfaces as follows:

$$N_r = \mp \frac{1}{16} m_p D \ddot{z} \left(1 + \frac{m_s}{m_p}\right) \frac{D}{H} \left[\frac{3+\nu}{4}\left(1 - \frac{4r^2}{D^2}\right) + (1+\nu)\ln\frac{2r}{D}\right]$$

$$N_\phi = \mp \frac{1}{16} m_p D \ddot{z} \left(1 + \frac{m_s}{m_p}\right) \frac{D}{H} \left[\frac{5\nu - 1}{4} - \frac{1+3\nu}{4}\frac{4r^2}{D^2} + (1+\nu)\ln\frac{2r}{D}\right]$$

where D and H are the diameter and depth of the dish, r is the radial coordinate, $\ddot{z}$ is the acceleration, m_p is the mass per unit area of the nonstructural payload (the mesh for the antennas under consideration herein) and m_s is the mass per unit area of the structure. Note that Poisson's ratio ν is equal to 1/3 for equilateral triangular lattices.

For the upper surface, an additional uniform isotropic compression induced by the mesh itself must be added to the foregoing acceleration-induced loads.

The shear load resultant, which must be carried by the inter-surface struts, is

$$Q_r = \frac{m_p D\ddot{z}}{4}\left(1+\frac{m_s}{m_p}\right)\left(\frac{2r}{D}-\frac{D}{2r}\right)$$

For the geodesic dome, assume that the thrust is applied at the feed position and is carried into the reflector structure through the rim. Then the radial and circumferential stress resultants in the dome surface are:

$$N_r = -m_p D\ddot{z}\left(1+\frac{m_s}{m_p}\right)\frac{F}{D}\left(1+\frac{r^2}{16F^2}+\frac{r^4}{128F^4}\right) - N$$

$$N_\phi = -m_p D\ddot{z}\left(1+\frac{m_s}{m_p}\right)\frac{F}{D}\left(1-\frac{5}{16}\frac{r^2}{F^2}-\frac{3}{128}\frac{r^4}{F^4}\right) - N$$

where F is the focal length. Note that this expression includes the additional loading N induced by the mesh.

For the triangular lattices under consideration herein, these surface loadings can be converted into design loads on the individual structure members. The strut loadings are dependent on the orientation of the triangular lattice with respect to the principal directions of loading. Thus, the strut compression is

$$P = -\frac{\sqrt{3}}{3}\ell\left[\frac{N_r+N_\phi}{2}+(N_r-N_\phi)\cos 2\alpha\right]$$

where α is the angle between the member and the direction of N_r. The maximum compressive load is given by $\alpha = 0$ or $\pi/2$ and is

$$P = \frac{\sqrt{3}}{3}\ell\left[|N_r-N_\phi| - \frac{N_r+N_\phi}{2}\right]$$

For the geodesic dome, the resulting worst-orientation strut loads are as shown in Figure 11. For the tetrahedral truss, the worst-orientation strut loads due to acceleration are shown in Figure 12. Note that in the case of the geodesic dome, the loading is dependent on the focal-length-diameter ratio both explicity in the equation and in the parameter C.

The compressive loads in the intersurface struts are also dependent on their orientation. The worst-orientation load is

$$P = \frac{\ell m_p D\ddot{z}}{4}\left(1 + \frac{m_s}{m_p}\right)\sqrt{1 + \frac{1}{3}\frac{\ell^2}{H^2}}\left(\frac{2r}{D} - \frac{D}{2r}\right)$$

STRUT SIZING

Each strut is assumed to be a thin-walled hollow tube with a wall thickness t and is designed to carry the compression load P as an Euler column with a factor of safety of F.S. The resulting diameter-to-length ratio of that strut is

$$\frac{d}{\ell} = \left(\frac{8F.S.}{\pi^3}\frac{P}{t\ell E}\right)^{1/3}$$

where E is Young's modulus. The mass per unit area of a single surface of these struts is

$$\frac{\text{Mass}}{\text{Area}} = 4\sqrt{3}\, k\rho\left(F.S.\frac{Pt^2}{E\ell}\right)^{1/3}$$

where ρ is the density of the strut material and k is a factor which is introduced to include the mass of the fittings.

Conceptually, it would be possible to design each separate strut with a proper diameter to carry the loading at its particular location and orientation. From a practical point of view, the fabrication problems involved in having many different sizes of

members are undesirable. Therefore, in the results herein, the assumption is made that all members are the same for the geodesic dome, for example. Thus the struts are designed to carry the maximum compression loads at the rim.

For the tetrahedral truss, the upper surface struts have the maximum loading at about the 80-percent radial station. It is assumed that all upper surface members are sized to carry this load. On the lower surface, the same size of struts are used as those of the upper surface unless the loading gets higher than their design load. As the center is approached, therefore, larger struts will be required. They are assumed to be all sized in accordance with the loading at the 5-percent radial station. The structure inboard of that station is considered to be thrust structure which is specially designed and is part of the propulsion system. Finally, the intersurface struts are assumed to have the same cross section as the lower surface struts.

Of course, the foregoing procedure of designing for compression is based on the assumption that tension strut loads are easily carried so that they have no effect on the design. This is indeed the case for such lightly loaded structures.

DESIGN MASS AND STOWAGE VOLUME

For the geodesic dome and the tetrahedral truss structure, the structural mass per unit area for the zero-acceleration case is

$$(m_s)_0 = 4\sqrt{3}\rho\left(\frac{\sqrt{3}}{3}\frac{Nt^2}{E}\,F.S.\right)^{1/3} \quad \text{(Geodesic Dome)}$$

$$= 4\sqrt{3}\rho\left(\frac{\sqrt{3}}{3}\frac{Nt^2}{E}\,F.S.\right)^{1/3}\left(2+\sqrt{\frac{1}{3}+\frac{H^2}{\ell^2}}\right)\text{(Tetrahedral Truss)}$$

The stowage length for "standard" packaging in which each strut is hinged in the middle is nominally $\lambda/2$ for the geodesic dome and $\ell + \sqrt{\ell^2/3 + H^2}$ for the tetrahedral truss.

The ratio of stowage diameter to deployed diameter is $3d/\ell$ for the "standard" packaging. In order to avoid problems from nonuniformities, it should be assumed that the joints are constructed with the outer diameter of the largest strut even when used with smaller struts.

INFLUENCE OF INTERORBIT ACCELERATION

Results for the increase in average mass per unit area and stowage diameter ratios are shown in Figure 13 for the geodesic dome and Figure 14 for the tetrahedral truss. For these examples, the required reflector mesh tension is assumed to 2.5 N/m (the geometric mean of 1.75 x 3.5 N/m, see ref. 2) and a support-tendon multiplier of 10 is used. Thus, N = 25 N/m. The tube wall thickness is selected to be 0.35 mm, the factor of safety to be 2, and the fitting factor to be 1.5. The material is assumed to be graphite/epoxy with a modulus of 110×10^9 N/m^2 and a density of 1520 kg/m^3, with a resulting structural unit mass as given in the figures. In the case of the tetrahedral truss, the depth and the surface-strut length are assumed to be equal and of the value shown in Figure 14, which is appropriate to a surface-accuracy budget of 10^{-5}.

In Figures 13 and 14, the unit structural mass and the diametral stowage ratio are given as a function of the interorbit acceleration for several diameters. The geodesic dome is very tolerant of acceleration, probably because the rim is used to distribute the load. Note that the results are for the dome portion only and do not include the mass or stowage volume for the rim.

The tetrahedral truss exhibits great sensitivity. Even the "small" 100-m-diameter reflector suffers a 50-percent increase in structural mass and a 100-percent increase in stowage diameter at

an acceleration of 1 m/sec^2. Note, however, that the packaged 100-m dish still weighs less than 2300 kg and has a diameter of 3.5 meters and a length of 7.6 m.

The results, of course, are only illustrative. No attempt has been made to seek high structural efficiency. A considerable reduction in the influence of acceleration could be attained simply by tailoring the strut selection to its particular orientation, even if only two sizes were used. Even more reduction could be achieved by using more than two sizes.

Similarly the simplest of basic strut designs has been used. The structure is heavy. For the tetrahedral truss, it is more than three times the weight of the payload (the mesh). Obvious potential exists for weight reduction.

REFERENCES

1. Powell, R.V.: Introduction to Large Space Antenna Session of Workshop on Space Radio Astronomy, Charlottesville, Virginia. JPL Internal Paper, 27 June 1979.
2. Montgomery, D.C.; and Sikes, L.D.: Development of the Maypole (Hoop/Column) Deployable Reflector Concept for Large Space Systems Applications. Large Space Systems Technology - 1979 Technology Review, Hampton, Virginia. NASA Conference Publication 2118, 7-8 November 1979.
3. Hedgepeth, J.M.: Accuracy Potentials for Large Space Antenna Structures. ARC-R-1014, Astro Research Corporation, 9 May 1980.

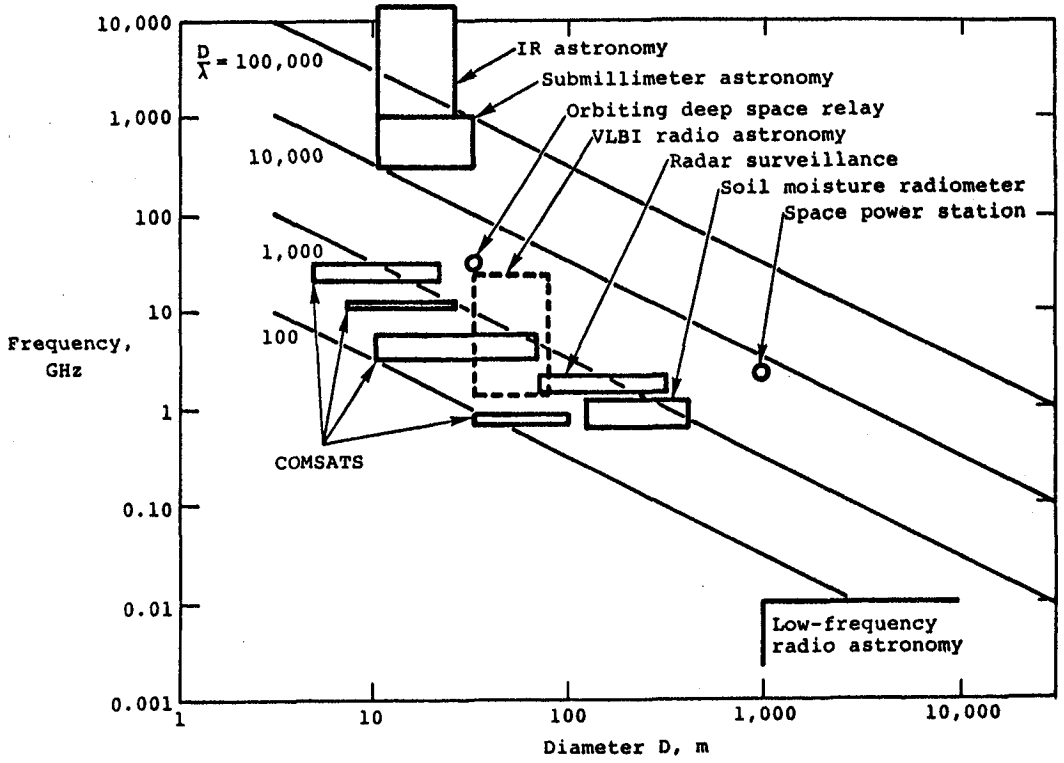

Figure 1. Large space antenna requirements.

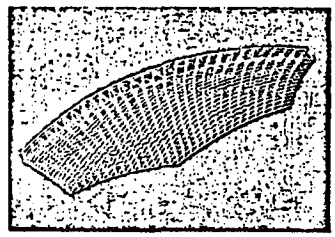

Tetrahedral truss

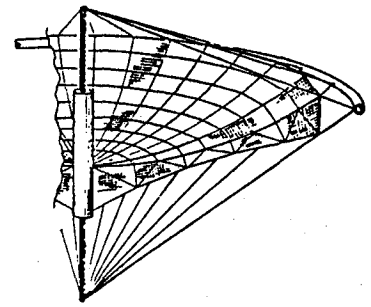

Pretensioned truss

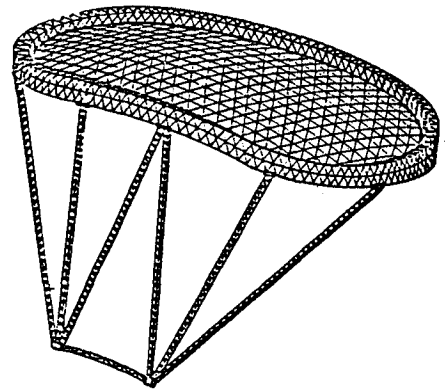

Orbiting reflector antenna

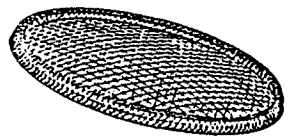

Geodesic dome

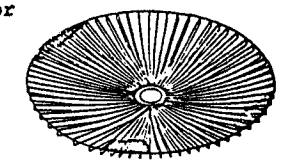

Radial rib

Figure 2. Antenna structural configurations for mesh-type reflectors.

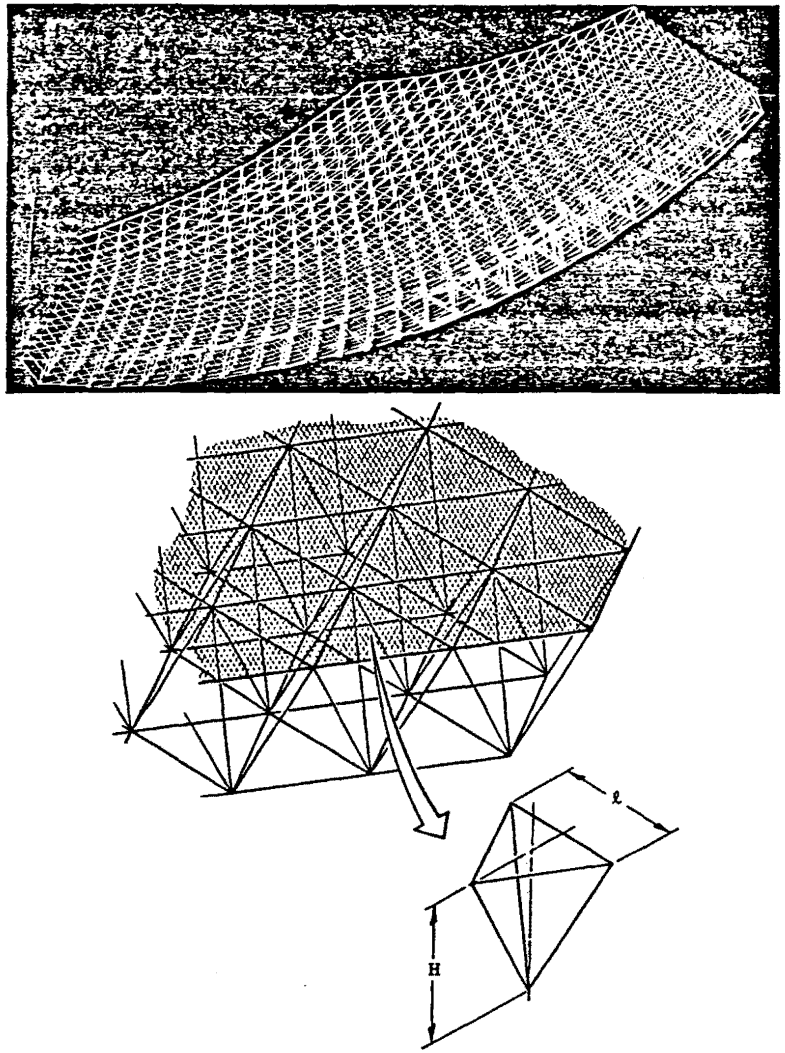

Figure 3. Tetrahedral-truss configuration.

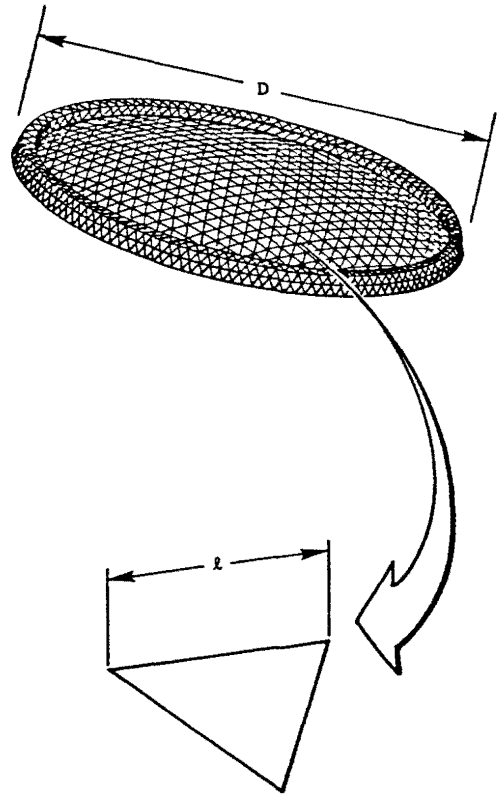

Figure 4. Geodesic-dome configuration.

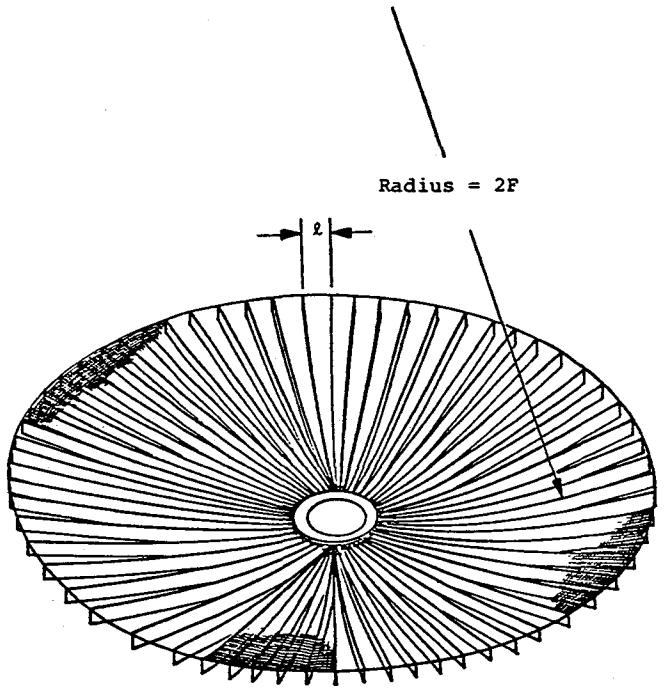

Figure 5. Radial-rib configuration.

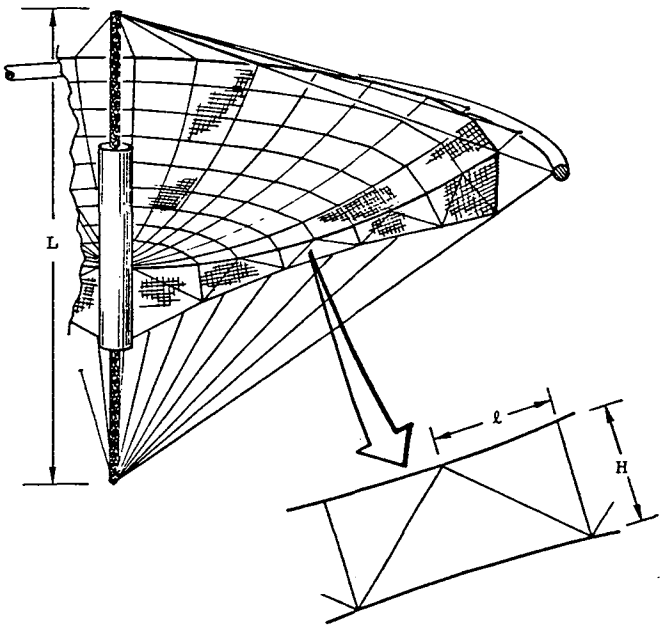

Figure 6. Pretensioned-truss configuration.

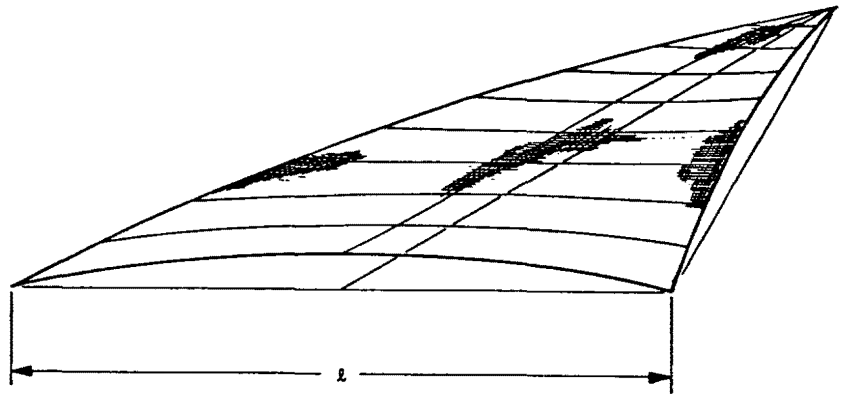

Triangular facet

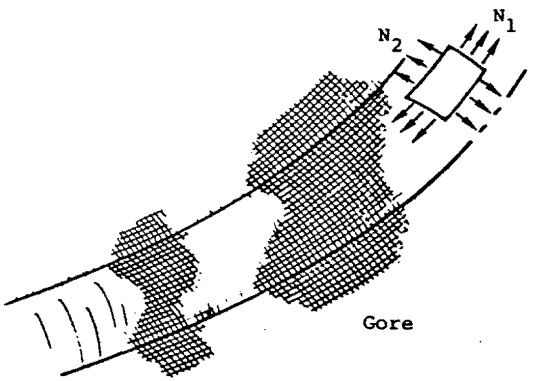

Figure 7. Mesh saddling.

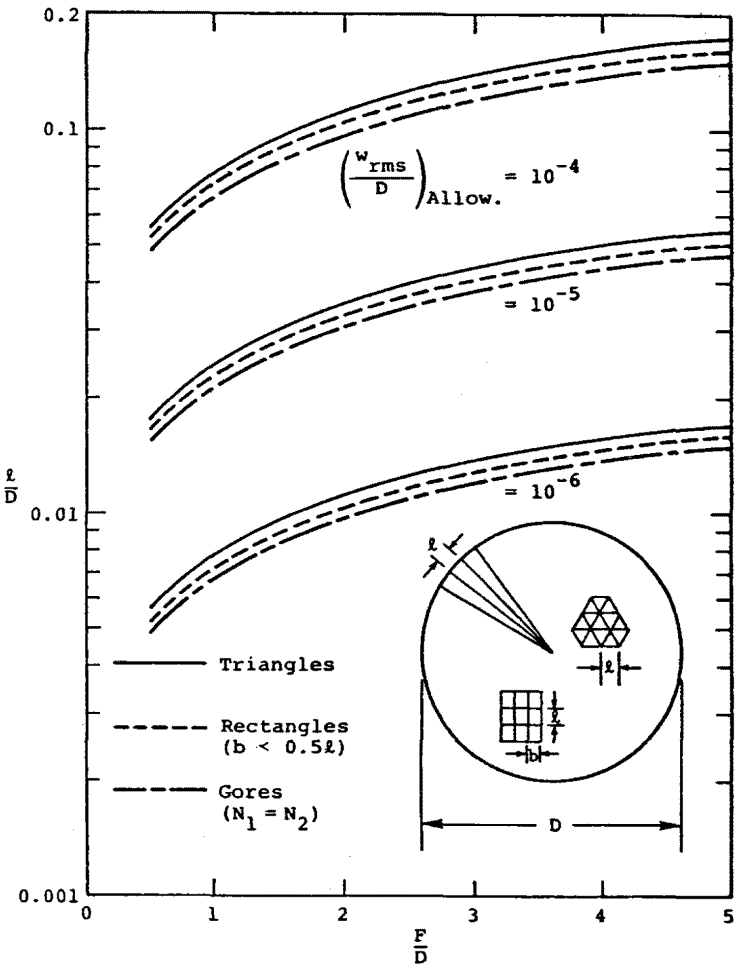

Figure 8. Influence of focal-length ratio and allowable surface error on size of mesh panels.

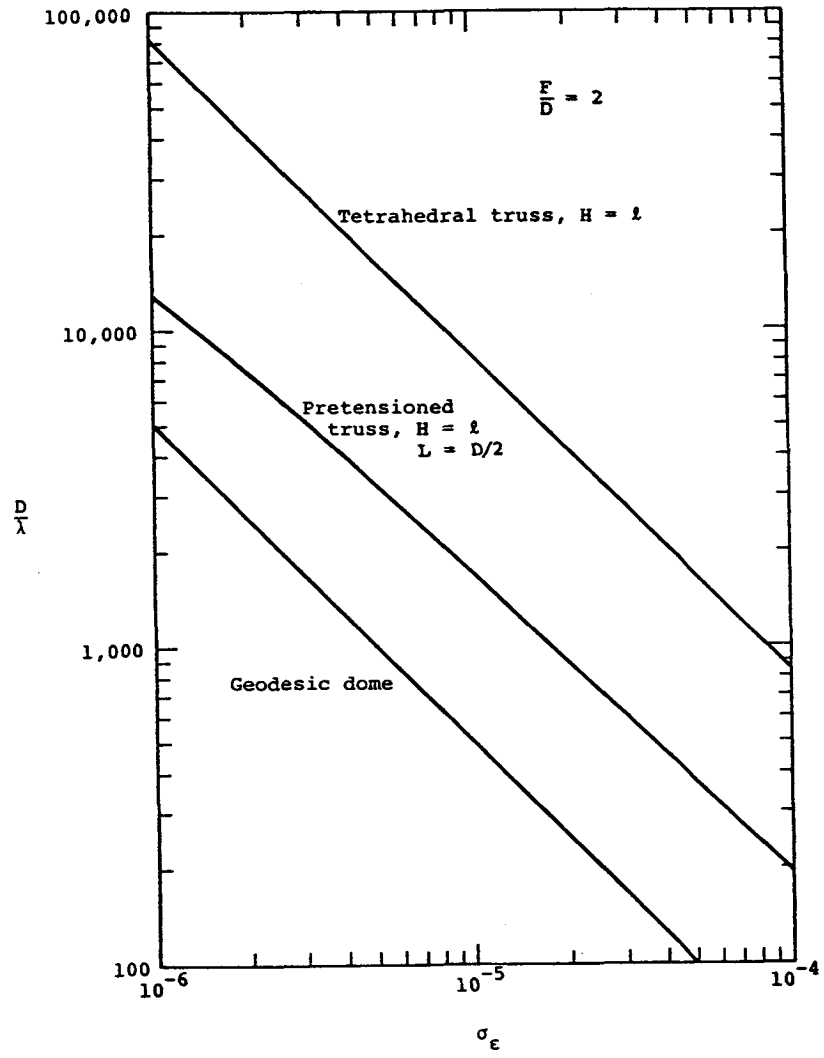

Figure 9. Potential antenna sizes for $w_{rms} = \lambda/100$ as limited by fabrication imperfections.

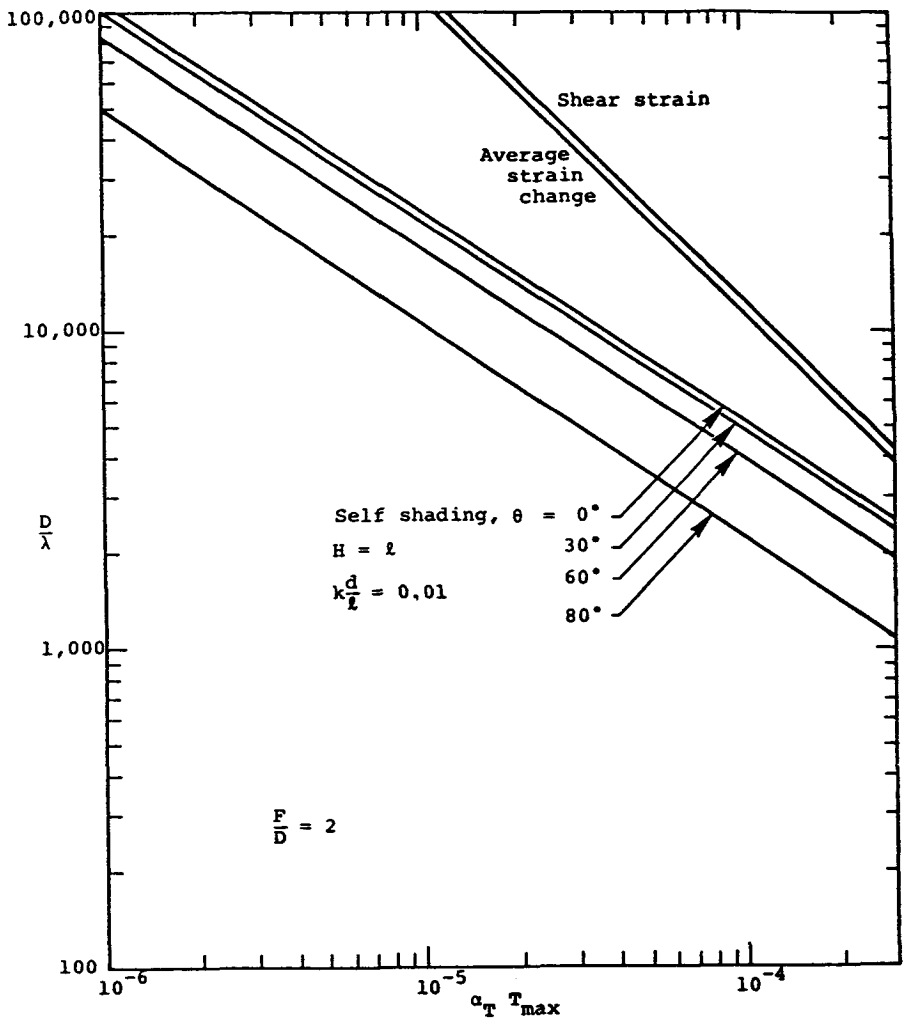

Figure 10. Potential tetrahedral-truss antenna sizes for $w_{rms} = \lambda/100$ as limited by thermal strains.

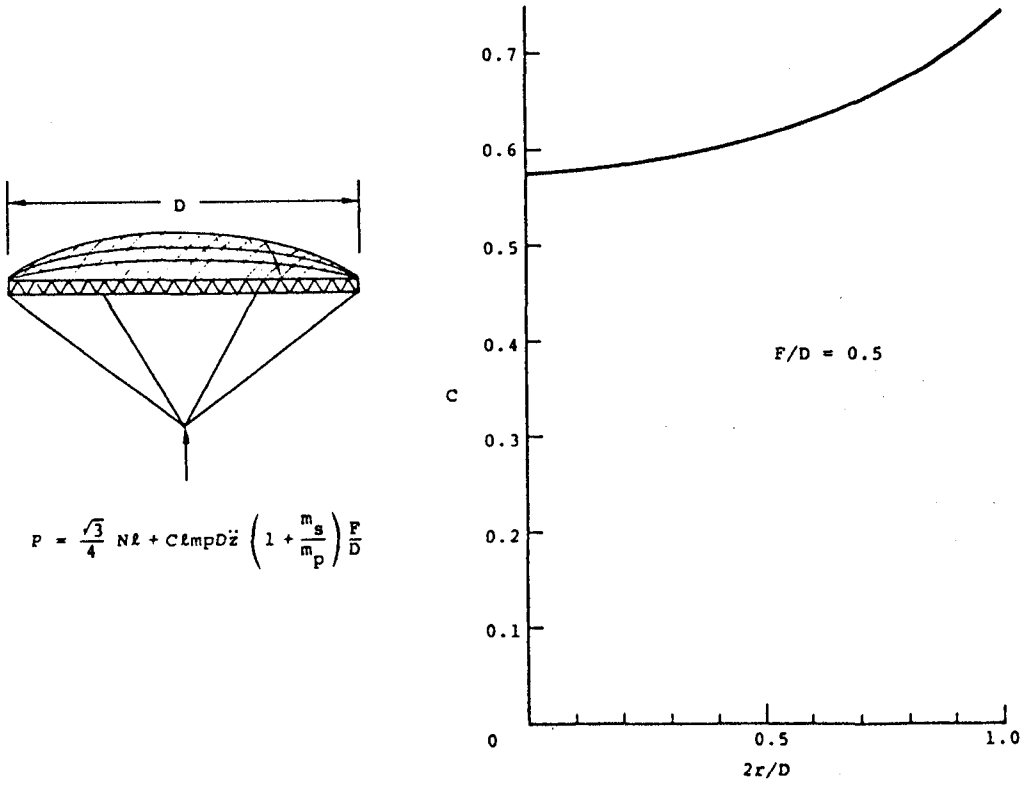

Figure 11. Strut loads in geodesic dome.

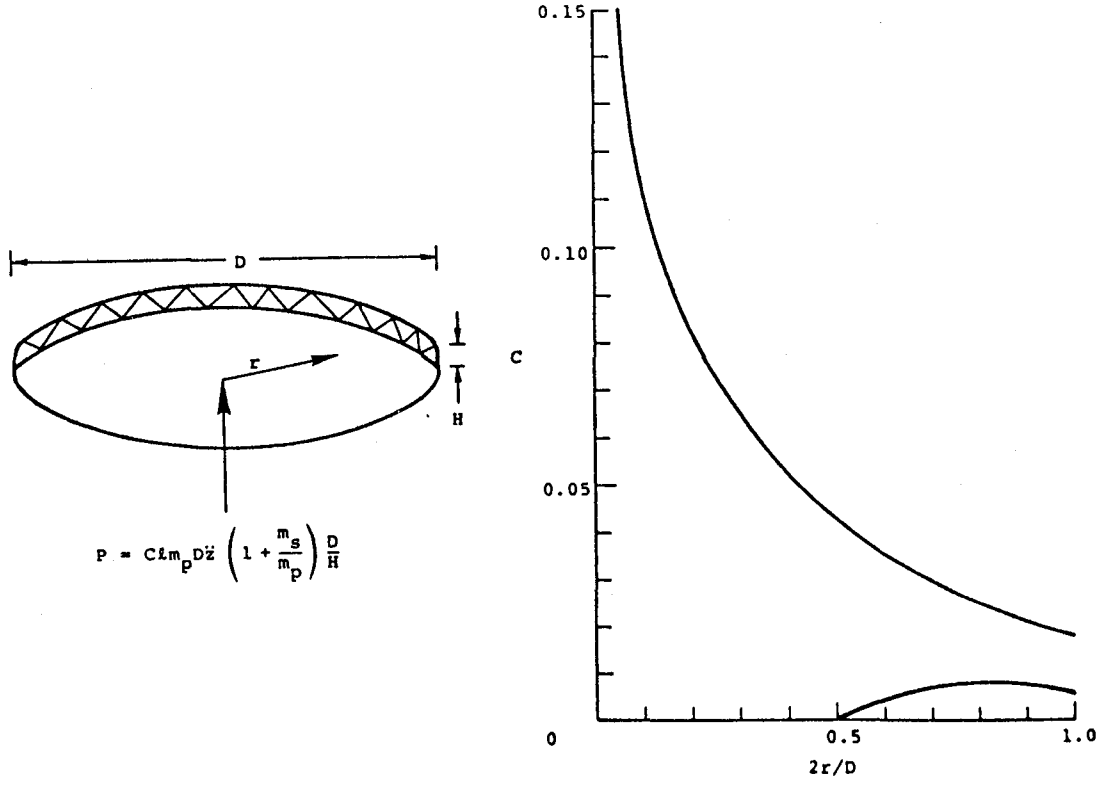

Figure 12. Strut loads due to acceleration - tetrahedral truss.

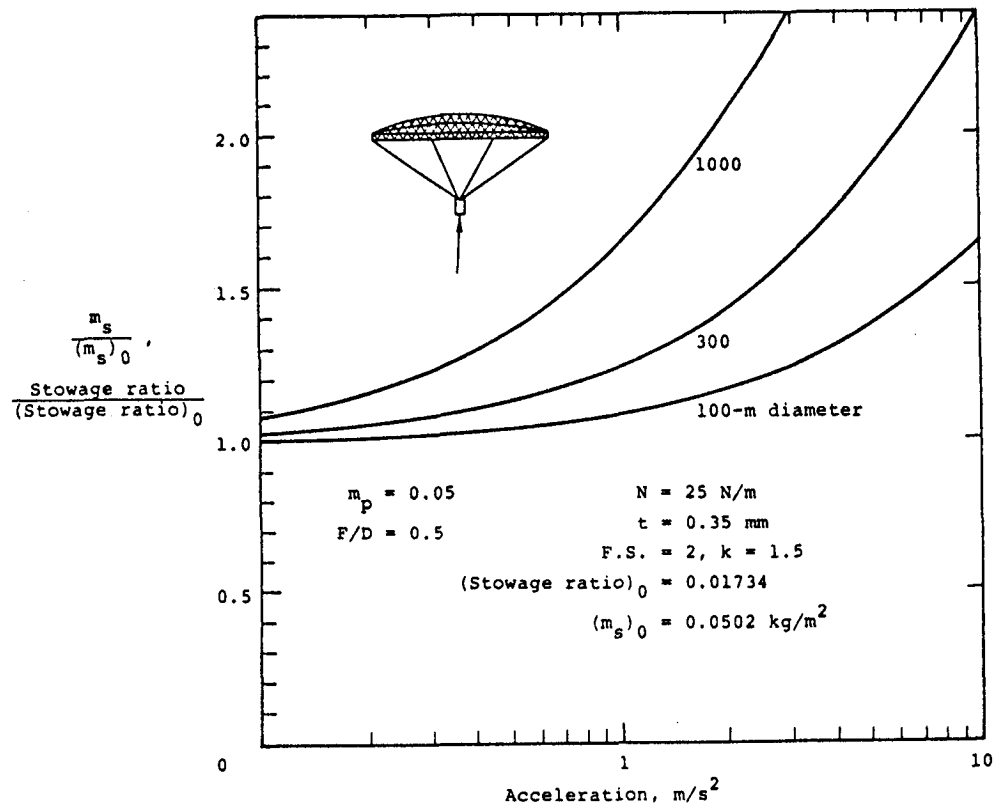

Figure 13. Mass and stowage ratio for geodesic dome.

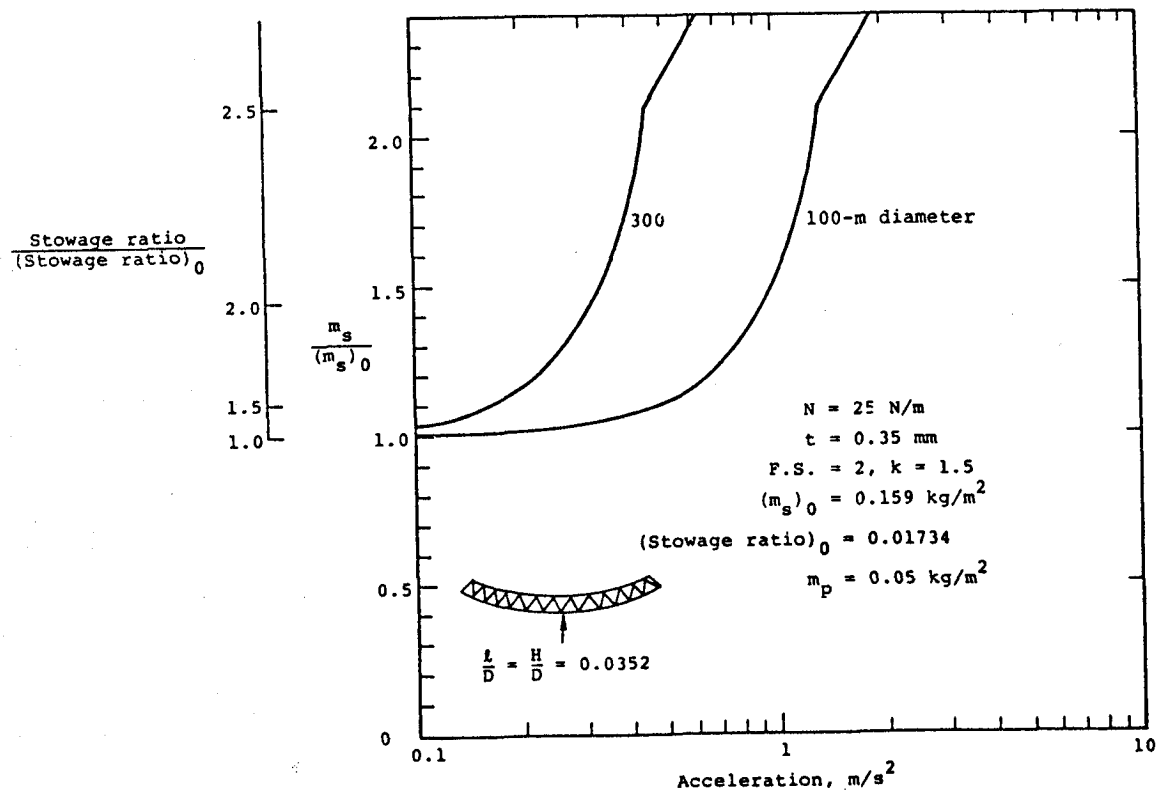

Figure 14. Mass and stowage ratio for tetrahedral truss.